

Tracking Single Particles and Elongated Filaments with Nanometer Precision

Felix Ruhnaw,^{†‡} David Zwicker,[§] and Stefan Diez^{†‡*}

[†]B CUBE—Center of Innovation Competence, Technische Universität Dresden, Dresden, Germany; [‡]Max Planck Institute of Molecular Cell Biology and Genetics, Dresden, Germany; and [§]Max Planck Institute for the Physics of Complex Systems, Dresden, Germany

ABSTRACT Recent developments in image processing have greatly advanced our understanding of biomolecular processes *in vitro* and *in vivo*. In particular, using Gaussian models to fit the intensity profiles of nanometer-sized objects have enabled their two-dimensional localization with a precision in the one-nanometer range. Here, we present an algorithm to precisely localize curved filaments whose structures are characterized by subresolution diameters and micrometer lengths. Using surface-immobilized microtubules, fluorescently labeled with rhodamine, we demonstrate positional precisions of ~2 nm when determining the filament centerline and ~9 nm when localizing the filament tips. Combined with state-of-the-art single particle tracking we apply the algorithm 1), to motor-proteins stepping on immobilized microtubules, 2), to depolymerizing microtubules, and 3), to microtubules gliding over motor-coated surfaces.

INTRODUCTION

Automated data analysis plays an essential role in collecting statistically significant amounts of information about biological processes. Furthermore, computational methods have greatly enhanced conventional microscopy methods and allow investigating the functions of biological molecules down to the nanometer level. For example, the point-spread-function (PSF) of well-separated subresolution particles can be evaluated by different algorithms, most commonly by centroid (center-of-mass) estimation, sum-absolute difference calculation, cross correlation, or by approximating the PSF with a two-dimensional (2D) Gaussian distribution (1). Using the latter, it has been shown that the localization precision of fluorescent probes is only limited by the number of photons collected (2). Among other applications, the localization of individual dye molecules with 1.5 nm precision (3) and the detection of 4 nm steps in cargo movement by the collective operation of kinesin-1 motors (4) has been achieved. Combining this method with photoswitchable fluorophores also led to the development of super-resolution techniques (5), which practically overcome the diffraction limit. Unfortunately, these single-particle tracking methods cannot analyze the position and dynamics of elongated filaments, such as actin filaments (6) or microtubules (7).

In filament assays, which are important tools to study the function of molecular motors *in vitro* (8), position or length measurements of filaments are still commonly analyzed manually (9). Another option is the manual evaluation of kymographs (10), temporal-spatial representations of an image sequence along a predefined path. First attempts of automatic tracking algorithms for filaments use methods

like center-of-mass calculation (11,12) or cross correlation (13) to follow filaments in an image sequence, but a change in shape of curved filaments can severely distort the measurements. More recent methods include path reconstruction (14) and open active contour models (15), which are able to find the filaments even at low signal/noise ratio, but are not able to automatically localize the filaments with precision below the pixel size. The first approaches to detect fluctuations of the filament centerline with nanometer precision have been undertaken by fitting one-dimensional (1D) functions, in particular Polynomials (16) or Gaussians (17), perpendicular to the filament, or by calculation of the sum-square difference (18). Recently, 1D Gaussian fitting has been used for semiautomated microtubule tip tracking with an accuracy of 36 nm *in vivo* (19). However, because all 1D methods require a transformation of the image data (including interpolation) their results may be influenced by the orientation of the filament.

Here, we present an algorithm capable of localizing the centerlines and the tips of curved (possibly crossing) filaments with nanometer precision. We combined our algorithm with single-particle tracking methods to create a so-called Fluorescence Image Evaluation Software for Tracking and Analysis (FIESTA) (see the MATLAB source code in the [Supporting Material](#)). The software includes further analysis tools like drift correction, color offset calculation, path statistics, and mean-square-calculation. We demonstrate the precision of our algorithm on fluorescently-labeled microtubules.

MATERIALS AND METHODS

Microtubule polymerization

Taxol-stabilized microtubules were grown for 30 min at 37°C from a 6.25 μ l BRB80 (80 mM Pipes (Sigma, St. Louis, MO), pH 6.9 adjusted with KOH

Submitted August 25, 2010, and accepted for publication April 11, 2011.

*Correspondence: diez@bcube-dresden.de

Editor: Xiaowei Zhuang.

© 2011 by the Biophysical Society
0006-3495/11/06/2820/9 \$2.00

doi: 10.1016/j.bpj.2011.04.023

(Merck, Darmstadt, Germany), 1 mM EGTA (Sigma), 1 mM MgCl₂ (Merck) solution supplemented by 2 μM tubulin (66% unlabeled bovine, 33% Rhodamine labeled bovine, Cytoskeleton, Denver, CO), 4 mM MgCl₂ (Merck), 1 mM Mg-GTP (Sigma), and 5% DMSO (Sigma). After polymerization, a volume of 494 μl BRB80T (BRB80 supplemented by 1 μM taxol (Sigma)) was added for further stabilization. 200 μl of the microtubule solution was centrifuged in a Beckman Airfuge (A95 rotor) at 100,000 × *g* for 5 min. The pellet was resuspended in a volume of 200 μl BRB80T. GMP-CCP-stabilized microtubules were grown for 2 h at 37°C from a 80 μl BRB80 (80 mM Pipes (Sigma), pH 6.9 adjusted with KOH (Merck), 1 mM EGTA (Sigma), 1 mM MgCl₂ (Merck)) solution supplemented by 2 μM tubulin (66% unlabeled bovine, 33% Rhodamine labeled bovine; Cytoskeleton, Denver, CO), 1 mM GMP-CPP (Jena Bioscience, Jena, Germany) and 1 mM MgCl₂ (Merck). 70 μl of the microtubule solution was centrifuged in a Beckman Airfuge (see above). The pellet was resuspended in a volume of 200 μl BRB80. Double-stabilized microtubules were grown like GMP-CCP-stabilized microtubules, but the pellet was resuspended in a volume of 200 μl BRB80T for further stabilization. The microtubule solution was diluted fourfold and centrifuged again.

Proteins

Full-length *Drosophila melanogaster* kinesin-1 was expressed in *Escherichia coli* and purified using the published protocols by Hancock and Howard (20). BCCP-rKin430GFP is a fusion protein that combines the C-terminal of the biotin carboxyl-carrier-protein (BCCP) with the N-terminal of a truncated kinesin-1. BCCP, a subunit of *E. coli* acetyl-coA-carboxylase can covalently bind biotin via lysin. Streptavidin-coated particles (e.g., quantum dots (QDs)) can then directly bind to the motor domain of the kinesin. As template for the motor protein, a truncated construct of rat kinesin-1 with an additional GFP (rKin430GFP; Rogers et al. (21)) was used. BCCP (300 bp) was isolated from the biotinylated kinesin construct K612-Bio (Berliner et al. (22)). Both fragments were fused using the overlap extension polymerase chain reaction method and expressed in *E. coli* in the presence of additional biotin (Sigma). Human MCAK-His6 was expressed in *Spodoptera frugiperda* (Sf9) cells (BAC-TOBAC expression system; Invitrogen, Carlsbad, CA), purified by cation-exchange, metal-chelating, and desalting or gel-filtration chromatography (23).

Microtubule and kinesin-1 assays

Surface immobilization of microtubules

We performed the experiments in flow channels, self-built (24) from two glass coverslips (22 × 22 mm² and 18 × 18 mm²; Corning, Inc., Corning, NY), which were cleaned in piranha solution (H₂O₂/H₂SO₄, 3:5; both Sigma) before silanization with 0.05% dichlorodimethylsilane in trichloroethylene (Sigma) and glued together by heated pieces of Parafilm M (Pechiney Plastic Packaging, Chicago, IL). The flow sequence was as follows: 1), The flow cell was filled with a solution of TetraSpeck microspheres (diameter 200 nm; Invitrogen) diluted 20-fold in BRB80. 2), After 2 min, the solution was exchanged with a BRB80 solution containing 0.5 μM monoclonal anti-β-tubulin antibodies (clone TUB 2.1; Sigma). 3), After 5 min, the surface was blocked with a solution with 1% Pluronic F-127 (Sigma) in BRB80. 4), Double-stabilized microtubules, diluted fourfold to prevent crossing microtubules, were incubated for 5 min to bind to the tubulin antibodies. 5), Microtubule solution was finally replaced by the imaging solution (BRB80 supplemented by 1 μM taxol, 20 mM glucose, 20 μg/ml glucose oxidase, 8 μg/ml catalase, 10 mM DTT; all from Sigma).

Stepping assay of QD-labeled kinesin-1

Tracking of GFP-labeled kinesin-1 motor proteins moving on immobilized microtubules has been previously described in Korten et al. (25). We immo-

bilized double-stabilized microtubules as described before and added 3 μl of a QD-kinesin mix to the imaging buffer supplemented by 0.2 μM ATP. The mix contained 3 μl of 10 nM streptavidin-coated QDs (Qdot 705 ITK Streptavidin Conjugate; Invitrogen) that were incubated with 3 μl of 0.06 μg/ml BCCP-rKin430GFP for 5 min.

Microtubule depolymerization

The assay is based on the experiments previously done by Helenius et al. (23). We immobilized GMP-CPP microtubules as described before and added 10 nM of the kinesin-13 MCAK.

Microtubule gliding assay

An extensive description of the microtubule gliding assay can be found in Nitzsche et al. (8), which also describes the Peltier element used for heating the flow cell.

Optical imaging

Fluorescence images were obtained using an inverted fluorescence microscope (Zeiss Axiovert 200M; Zeiss, Jena, Germany) with a 100× oil immersion objective (Zeiss APOCHROMAT NA 1.46; Zeiss) with an additionally 1.6× magnifying optovar. The final pixel size was 100 nm. Microtubules were observed by epifluorescence using a Lumen 200 metal arc lamp (Prior Scientific Instruments Ltd., Fulbourn, UK) with a TRITC (exc 535/50, em 610/75, dc 565 LP; all Chroma Technology, Rockingham, VT) filterset. QDs were observed by total internal reflection fluorescence microscopy using a mixed gas argon-krypton laser (Innova 70C Spectra; Coherent, Santa Clara, CA) with a customized Qdot705 (exc 488/10, dc 488RDC; both Chroma; em BL710/40; Semrock, Rochester, NY) filterset. Image acquisition was performed with 100 ms exposure in streaming mode by an electron-multiplied charge-coupled device camera (iXon DV 897; Andor, Belfast, Northern Ireland) in conjunction with a Metamorph imaging system (Universal Imaging Corp., Downingtown, PA).

Image processing

The algorithm was implemented in MATLAB (The MathWorks, Natick, MA) and includes a graphical-user-interface for user initialization and data analysis after tracking. We used the `bwmorph()` function (image processing toolbox) for the thinning algorithm and the `lsqnonlin()` function (optimization toolbox) for solving the nonlinear least-square problem. For statistical analysis of the localization precision, we used the `mle()` function in the statistics toolbox for the maximum-likelihood-method.

ALGORITHM

Automated tracking algorithms analyze image sequences where multiple images of the same field of view are acquired in a temporally sequential manner. Each individual image of an image sequence consists of a given number of pixels associated with specific intensity values, represented for example by 8 bit (values of 0–255) or 16 bit (values of 0–65535) integers. Being derived from the digital conversion of the photons collected by the sensor chip on the front end of the camera, the intensity values are linearly related to the light intensity captured by the respective pixels. Typically, the intensity values are visualized by certain gray levels varying from black for the lowest intensity value to white for the highest intensity value. In fluorescence microscopy the objects of interest are labeled by fluorophores,

which emit light upon excitation and thus appear with higher intensity than the background.

Due to the limited resolution of an optical microscope, the captured signals of the objects (further on denoted as intensity profiles) are given by a convolution of the object with the PSF of the imaging system. Given that the pixel size should be at least a factor of two smaller than the lateral dimension of the PSF (26), the captured light of any object (even when being represented by just a single fluorophore) will spread over multiple pixels. Although a rough estimation of the position of such objects can be obtained by searching for the pixel with the highest intensity value, the localization precision can be significantly increased when all pixels of the intensity profile are included in the analysis. Image processing methods toward this aim include center-of-mass calculations or fitting the intensity profile to an approximation of the PSF. However, these methods fail if multiple emitters are in close proximity, creating more complex intensity profiles. For fluorescently labeled filaments characterized by subresolution diameters and micrometer lengths, we overcome this limitation by deriving a number of theoretical models based on the Gaussian distributions given by Eqs. 1–4.

Tracking algorithms that link the movement of objects into trajectories without user interaction, can be categorized into 1), feature-based tracking algorithms, where the objects are detected in every image individually and then linked into trajectories based on their features, or 2), region-based tracking algorithms, where image regions are matched to regions in other images by cross correlation. Whereas both methods can achieve subpixel precision when detecting the motion of particles and filaments, we find the feature-based tracking algorithm more versatile for our applications, which involve tracking the exact shapes of filaments. Furthermore, by analyzing every image independently, parallel processing on multiprocessor systems and clusters is possible.

After user initialization (where a number of parameters can be set manually), the tracking algorithm first evaluates every image in an image sequence independently (Fig. 1) and then links the detected objects into trajectories using a graph-theoretic approach. The first part of the algorithm is characterized by the following five steps: Thresholding, Feature detection, Image segmentation, Fitting process, and Interpolation.

EQUATIONS 1–4

$$I_1(x, y) = \frac{1}{2\pi\sigma_x\sigma_y\sqrt{1-\rho^2}} \cdot \exp \left[-\frac{1}{2(1-\rho^2)} \left(\left(\frac{x-\hat{x}}{\sigma_x} \right)^2 - 2\rho \left(\frac{x-\hat{x}}{\sigma_x} \right) \left(\frac{y-\hat{y}}{\sigma_y} \right) + \left(\frac{y-\hat{y}}{\sigma_y} \right)^2 \right) \right] \quad (1)$$

$$I_2(x, y) = \frac{1}{2\pi\sigma^2} \cdot \exp \left[-\frac{(x-\hat{x})^2 + (y-\hat{y})^2}{2\sigma^2} \right] \quad (2)$$

$$I_3(x, y) = \frac{\zeta}{2\pi\sigma_c^2} \cdot \exp \left[-\frac{(x-\hat{x})^2 + (y-\hat{y})^2}{2\sigma_c^2} \right] + \frac{1-\zeta}{(2\pi)^{3/2}r\sigma_r} \cdot \exp \left[-\frac{\left(\sqrt{(x-\hat{x})^2 + (y-\hat{y})^2} - r \right)^2}{2\sigma_r^2} \right] \quad (3)$$

$$I_4(x, y) = \frac{1}{\sqrt{2\pi}\sigma^2} \cdot \frac{1}{l} \cdot \exp \left[-\frac{(- (x-\hat{x}) \cdot \sin \theta + (y-\hat{y}) \cdot \cos \theta)^2}{2\sigma^2} \right] \quad (4)$$

Equation 1 represents a bivariate normal distribution or 2D Gaussian distribution, which is a generalization of a univariate normal distribution to two dimensions. The \hat{x} and \hat{y} denote the center of the peak, σ_x^2, σ_y^2 the variance in x and y direction, and ρ the correlation coefficient between the x and y direction. **Equation 2** is a symmetric bivariate normal distribution or symmetric 2D Gaussian distribution that is simplified from Eq. 1 using $\sigma = \sigma_x = \sigma_y$ and $\rho = 0$. **Equation 3** is adapted from Toprak et al. (27) where a Gaussian ring of radius r is added to a symmetric 2D Gaussian distribution, which can be used for tracking defocused single particles. The σ_c^2, σ_r^2 , denote the variance of the Gaussian distribution in the center and the Gaussian ring, respectively, and ζ weighs the relative contributions of the center peak to the ring. **Equation 4** represents a Gaussian wall, which is a generalization of the univariate Gaussian distribution perpendicular to a line. The l denotes the length of the Gaussian wall and θ the angle between the Gaussian wall and the x axis. Adapted transformations of these normalized functions, including an amplitude parameter and a background value, were used as models in our fitting process (see Section S.1 in the Supporting Material).

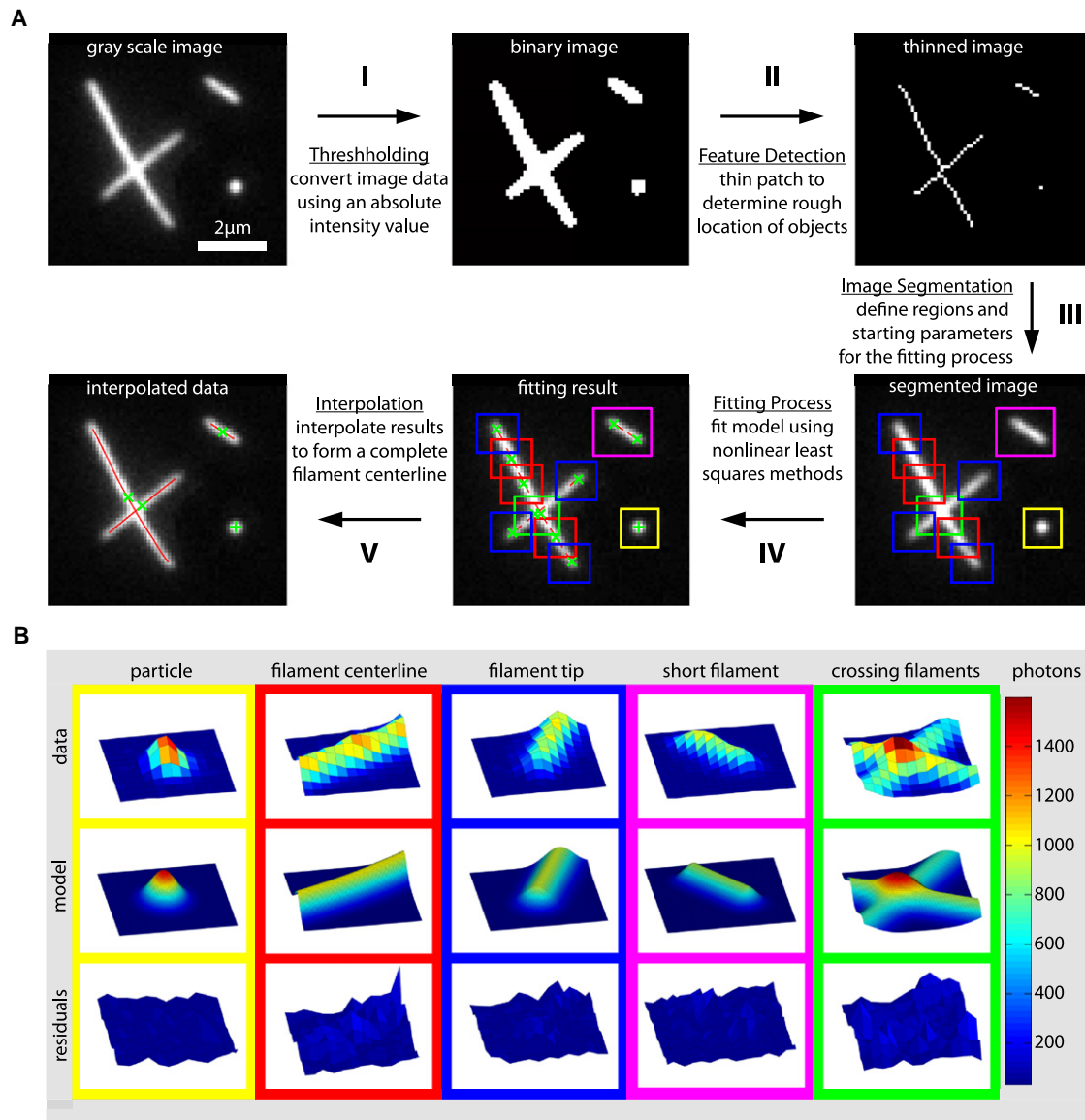


FIGURE 1 Algorithm for tracking individual frames containing filaments and individual particles: (A) Workflow of the tracking algorithm with corresponding images for every step. Plus (+) symbols denote the center positions of individual particles, whereas center positions of filaments and filament segments are marked with a cross (x). Red lines indicate the orientation of the model or the centerline of the filament. (B) Intensity profiles for different regions (colors correspond to regions in Fig. 1 A), the corresponding model, and the residuals after fitting.

Thresholding

To identify the objects to be analyzed, the gray scale images are first converted into binary images with pixel values of 1 (true) when the original intensity value was above a user-defined intensity threshold and 0 (false) otherwise. All true pixels having at least one neighbor (any of the surrounding pixels that have a true value) are connected to patches. Alternatively, an automated threshold algorithm using edge detection with different image operators and filling the detected edges with morphological operations on the binary image can be applied (see Section S.2 in the Supporting Material). Additional transformations, such as

averaging the intensity values in the original gray scale image by a kernel (size 3×3 pixel), can be optionally applied to improve the quality of the binary image.

Feature detection

Point objects (individual particles) are searched for in patches with an area below a user-defined patch area threshold. The rough locations of the individual particles are derived, after filtering the original intensity values in the patch area with a Wiener filter (size 3×3 pixel), from the positions of the local image maxima, each represented by a pixel that is exclusively surrounded by pixels with lower intensity values. Line

objects (filaments) are searched for in patches with an area above the user-defined patch area threshold. The rough centerlines of the filaments are determined by applying a thinning algorithm (28) to the patch. The resulting extended lines with the width of one pixel, or networks thereof, are then assigned to different filament features that only depend on the number of true pixel neighbors: 1), tip points have one neighbor, 2), centerline points have two neighbors, and 3), crossing points have more than two neighbors. If crossing points are present in a network, three or more lines will extend from the crossing points toward the tip points. The smallest angle between these lines then determines which true pixels belong to the same filament. Afterward, all detected features are assigned to individual filaments.

Filaments with a total number of pixels \tilde{n} are now represented by an ordered set of points (parametric curve) $\tilde{F}_p = (\tilde{x}_p, \tilde{y}_p)$, $p = (1, 2, \dots, \tilde{n})$ where \tilde{x}_p and \tilde{y}_p denote the pixel position of the true pixel with index p . The tip points, \tilde{F}_1 and \tilde{F}_n , are referred to as start and end points, respectively. Finally, the parametric curve \tilde{F}_p will be smoothed with a moving average filter of size $2\sigma + 1$ (rounded to an integer number of pixels), where σ denotes the user-defined scale estimation. The scale estimation σ characterizes the dimension of the image features to be localized. For filaments (or particles) it is derived from the measured full-width half-maximum of a linescan perpendicular to the filament (or across the particle) by $\sigma = FWHM/2\sqrt{2 \ln 2}$.

Image segmentation

The features detected are used to segment the image into quadratic regions. The side length, a , of these regions is chosen based on the scale estimation by $a = 8\sigma$ (rounded to an integer number of pixels). For point objects, the regions are placed around the rough location of the object with the brightest pixel in the center of the region. For line objects, regions are first placed around the rough locations of the tip and crossing points. The remaining centerline points are covered by additional regions. The distance d between the center points of these additional regions is chosen to be $d \sim 6\sigma$ allowing for an overlap of these regions. Finally, all regions that overlap more than 50% in area will be merged and treated as clusters. Clusters are consequently described by the sum of two or more theoretical models.

Fitting process

Every region that was created in the image segmentation is now analyzed individually. Thereby the original intensity profiles are approximated by numerical models (Fig. 1 B) based on Gaussian distributions (Eqs. 1–4, see Section S.1 in the Supporting Material) with only a limited set of parameters: background, center position, orientation, amplitude, width, and curvature. The starting values for these parameters are estimated as follows: 1), the initial background value is

set by the average intensity of all pixels in the region that are below the intensity threshold, 2), the initial center position of the model is given by the position of the region's center pixel, 3), the initial amplitude of the model is derived from the original image intensity value at the center position minus the background value, 4), the filament orientation at the center point of the region is determined by weighted averaging of the angles between this point and all other points of the filament, and 5), the width is given by the scale estimation σ .

The numeric models are compared to the original intensity profiles and their parameters are optimized by minimizing the sum of the squared residuals. Optimization is done with either a subspace trust-region method, which is based on the interior-reflective Newton method (29,30), or the Levenberg-Marquardt method (31,32), if the former fails. The algorithm can also calculate the errors of the parameters using the Jacobian matrix of the model (see Section S.3 in the Supporting Material).

Interpolation (only filaments)

For every filament, the algorithm connects the segments and computes a refined centerline with subpixel resolution. Therefore, a spline interpolation (see Section S.4 in the Supporting Material) is performed using piecewise third-order polynomials between consecutive segments defined by the position and orientation derived in the fitting process. We placed n points (approximately the length of one pixel apart) on the spline curve to represent the centerline $F_p = (x_p, y_p)$, $p = (1, 2, \dots, n)$. The length of the filament and its center position (X, Y) are determined by the distance along the curve between the two tips and the midpoint on the curve between the two tips, respectively.

The second part of the algorithm links all tracked objects in the image sequence into trajectories $T_k = (X_k, Y_k)$, $k = (1, 2, \dots, N)$ using a modified feature point tracking algorithm (33). To establish a temporal link between objects, we calculate a cost function, which includes features like center position, speed, direction of movement, and amplitude or length of the objects. Different weights can be assigned by the user to different features. All weights have to be between 0 and 1, and the sum of the weights has to equal 1. This way, linking the objects can be optimized including the merging of trajectories with partial occlusions. For example, direction and speed of movement can be given a large impact for a processively moving motor protein while these features are less relevant for a diffusing molecule. There, only the position (proximity) is of interest.

We tested the precision of our algorithm by analyzing an image sequence (500 frames) of immobilized fluorescently labeled microtubules (Fig. 2) in EPI-fluorescence (pixel

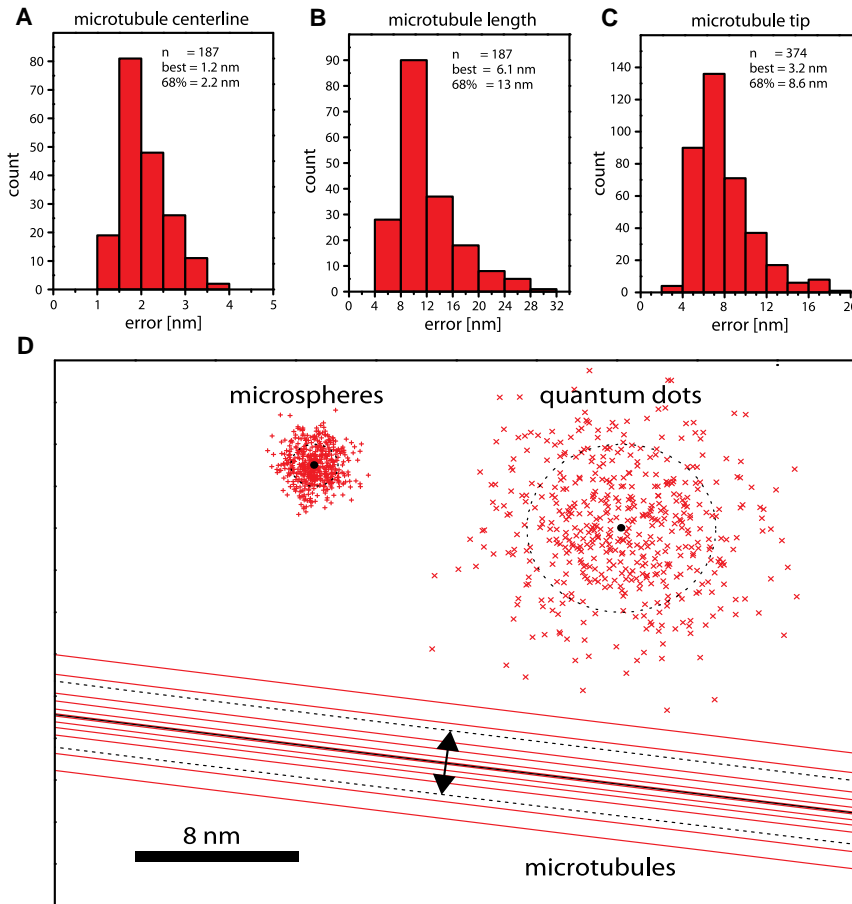


FIGURE 2 Precision (68% confidence interval) of filament tracking: The smallest error of the values shown in the histograms is denoted as best and the overall error of the microtubule distribution is denoted as 68%. (A) Histogram of microtubule centerline errors. (B) Histogram of microtubule length errors. (C) Histogram of microtubule tip position errors. (D) Centerline localization of one microtubule compared to center position localization of one TetraSpeck Fluorescent Microsphere (diameter 200 nm) and one Qdot 705 ITK Streptavidin Conjugate. Plus (+) and cross (x) symbols denote the center positions (500 frames) of the microsphere and the QD. The black dot indicates the centroid of the particles and the black dotted lines the 68% confidence interval of the particle's centroid measurement. The red lines denote the centerlines of the microtubule (11 of the 500 frames). The black line indicates the averaged microtubule centerline and the black dotted line the 68% confidence interval of the microtubule's averaged centerline measurement.

size 100 nm, exposure time 100 ms, continuous streaming acquisition mode). A total of 187 immobilized microtubules were tracked in different fields of view to get sufficient statistics on the precision. Additionally, we tracked the center positions of 10 microspheres in every field of view. Their average displacement was used to correct the tracked positions of the microtubule centerline for lateral drift. For each microtubule a number of characteristic errors were calculated: 1), The centerline error (see Sections S.5 and S.6 in the Supporting Material) is given by a value that includes at least 68% of all centerline deviations (Fig. 2 A). 2), The length error is given by the standard deviation of all tracked microtubule lengths (Fig. 2 B). 3), The tip error is calculated by the width of the 2D tip position distribution where we assumed a symmetric 2D normal distribution and estimated the width using the maximum-likelihood method (Fig. 2 C). The smallest error of the values shown in the histograms is denoted as “best” and the overall error of the microtubule distribution, denoted as “68%”, is defined by the error value that includes at least 68% of the tracked microtubules. Thereby we estimate a positional precision of 2.2 nm when determining the microtubule centerline and 8.6 nm when localizing the microtubule tips. The length measurements are mainly influenced by the tip error and we

estimate an overall length error of 13 nm. For illustrative purposes, we compared the centerline error of one tracked microtubule to the localization errors of a 200 nm large fluorescent microsphere and a Qdot705 quantum dot (Fig. 2 D).

Using simulated microtubules (see Section S.5 in the Supporting Material) at various signal/noise ratios, we compared our 2D filament tracking algorithm with an approach based on 1D fitting perpendicular to the filament (17). We found that our 2D tracking algorithm, which does not depend on any image rotation, generated more precise data and performed more than 10× faster (see Section S.7 in the Supporting Material).

APPLICATIONS

To demonstrate the high precision of the 2-D filament tracking, we present three possible applications (Fig. 3).

2D tracking of kinesin-1 motors on immobilized microtubules

Because microtubules consist of ~13 protofilaments their lattice represents an extended surface to motor proteins. To test if our algorithm can be applied to follow the stepping

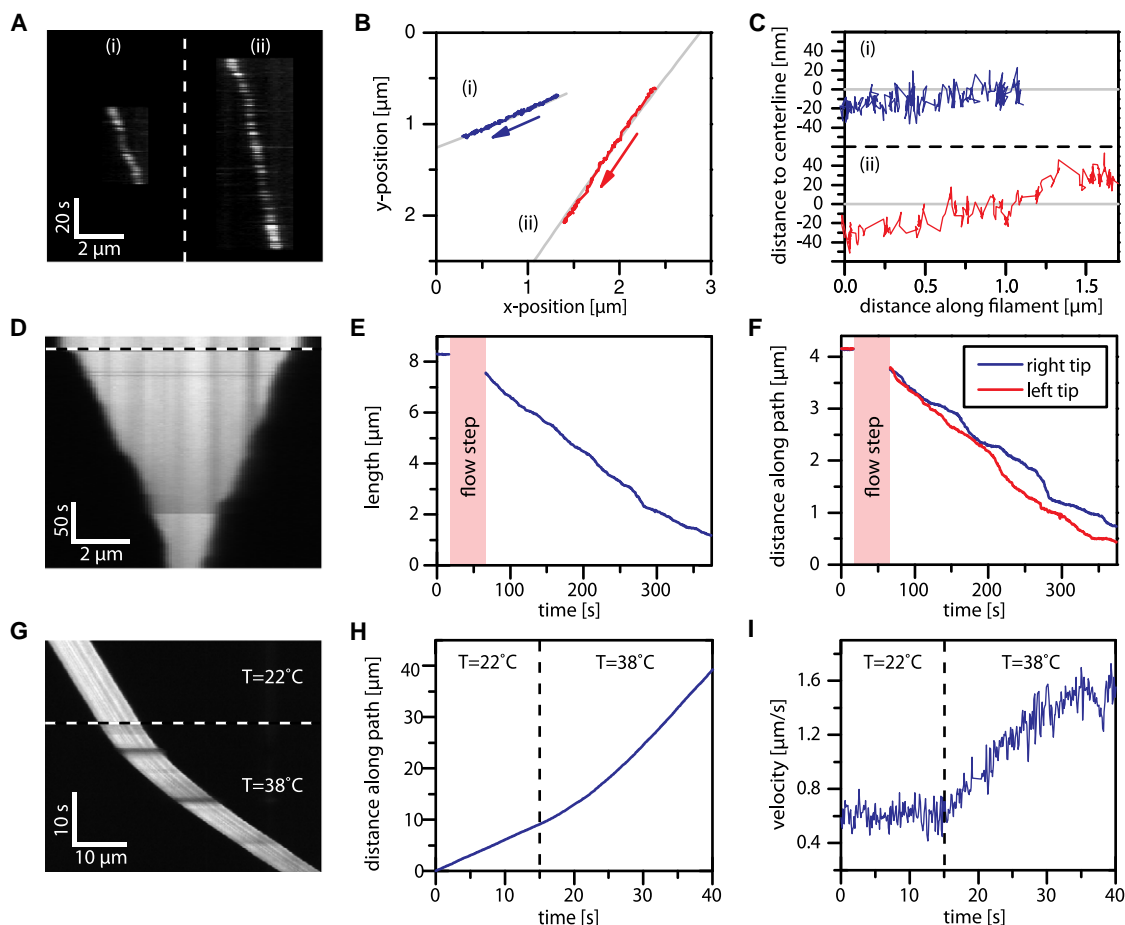


FIGURE 3 Applications of the filament tracking algorithm: (A) Kymograph of two QDs transported by kinesin-1. (B) Trajectory of both QDs and the centerline of their corresponding microtubules (gray). (C) Distance to the track for both QDs, gray denotes the microtubule centerline. Positive values denote the left hand side, negative the right hand side (in the direction of movement). (D) Kymograph of microtubule depolymerized by the kinesin-13 MCAK (10 nM concentration). The dotted line marks the time when the MCAK solution was flowed in. (E) Decrease in microtubule length due to depolymerization. (F) Movement of the microtubule tips in respect to the initial center position of the microtubule. (G) Kymograph of microtubule gliding over a kinesin-1 coated surface. The dotted line marks the time, when the temperature was increased from 22°C to 38°C (temperature of the Peltier element attached to the flow cell containing the motility solution). (H) Distance along the path of the microtubule center position. (I) Instantaneous velocity of the microtubule center position.

of processive kinesin-1 motors on the microtubule lattice in two dimensions, we immobilized rhodamine labeled microtubules on a glass coverslip via tubulin antibodies (25). We then added kinesin-1 motor proteins that were labeled with streptavidin-coated QDs (emission at 705 nm) bound to the biotinylated motor domain. In the presence of ATP, we acquired an image sequence (100 frames) of the microtubules in EPI-fluorescence and afterward imaged the movement of single QDs using total-internal reflection fluorescence microscopy (for both: pixel size 100 nm, exposure time 100 ms, continuous streaming acquisition mode). Ten Tetraspeck microspheres within the field of view (visible in both image sequences) were used for drift correction and for the correction of the color offset.

The persistent movement of kinesin-1 motors along two microtubules is shown by the QD kymographs in Fig. 3 A. Here, kymographs are space-time plots that display intensity

values along a predefined path (along the microtubule) over time. We overlaid the QD trajectories with the tracked microtubules (Fig. 3 B) and calculated the relative distance of the QDs to the averaged microtubule centerline (Fig. 3 C). Although we did not find any abrupt motion of the motors perpendicular to the microtubule centerline, we rather observed a nonparallel movement of the motors with respect to the microtubule centerline (see Section S.8 in the Supporting Material for more traces). This behavior is expected for kinesin-1; it follows individual protofilaments of super-twisted microtubules in a helical manner (34). In our case, the microtubules were grown in the presence of nonhydrolysable GTP analog GMP-CPP and most likely consisted of 14 protofilaments with a supertwist periodicity of $\sim 8 \mu\text{m}$ (8). Given the short run length of kinesin-1 (on average $1 \mu\text{m}$) the observation of a complete rotation of the QD around the microtubule was unlikely. None of the 43 tracked QDs

was localized more than 60 nm away from the averaged microtubule centerline. This is consistent with the molecular geometry in our assay when considering a size of ~ 5 nm for the kinesin-1 motor domain, ~ 10 nm for streptavidin, and ~ 20 nm for the QD diameter. With these values one estimates a maximum distance of the QD center from the microtubule (diameter ~ 25 nm) centerline of ~ 37 nm. So far, the helical movement of kinesin-1 on the microtubule has not been reported for this so-called stepping geometry and we are only able to resolve this movement due to the high precision measurement of the microtubule centerline.

Tracking the lengths of microtubules depolymerized by kinesin-13

In cells, microtubules are highly dynamic, i.e., alternating phases of filament polymerization and depolymerization can be distinguished. To test if our algorithm can be applied to measure the length of depolymerizing microtubules *in vitro*, we immobilized rhodamine labeled microtubules on a glass coverslip via tubulin antibodies and added kinesin-13 motor proteins (MCAK), which are known to depolymerize microtubules (23). In the presence of ATP, we acquired an image sequence of multiple microtubules in EPI-fluorescence (pixel size 100 nm, exposure time 100 ms, time lapse acquisition mode at 2 frames per second) before and after the addition of MCAK (indicated by flow step in Fig. 3, E and F). Ten Tetraspeck microspheres within the field of view were used for drift correction.

The kymograph of one shrinking microtubule is shown in Fig. 3 D. We plotted the tracked length of the microtubule in Fig. 3 E. Here, the high precision of the microtubule tracking reveals fluctuations in the depolymerization rate. When analyzing the movement of both microtubule tips individually (Fig. 3 F), different depolymerization rates become apparent (in accordance with (35)). So far, automated microtubule length measurements with nanometer precision have not been reported and we demonstrate that the high precision of our algorithm might help to reveal distinct shrinking characteristics being missed otherwise.

Tracking the gliding motion of kinesin-1 driven microtubules

In vitro gliding motility assays, where microtubules are propelled over a surface of immobilized motors, are important biophysical tools to study the behavior of single- and multimotor transport (8). To test if our algorithm can be applied to follow the motion of kinesin-1 driven microtubules, we unspecifically bound full-length kinesin-1 motors to a glass coverslip and added rhodamine labeled microtubules. In the presence of ATP, we acquired an image sequence of gliding microtubules in EPI-fluorescence (pixel size 100 nm, exposure time 100 ms, continuous streaming acquisition mode). During imaging we increased the

temperature of the solution from 22°C to 38°C , which led to an increase of the gliding velocity. Five Tetraspeck microspheres within the field of view were used for drift correction.

The linear movement, before and after the temperature increase, is shown by the kymograph (along the filament path) in Fig. 3 G. We calculated the distance D_k (see Section S.9 in the Supporting Material) of the center position along the path and plotted the displacement of the microtubule over time (Fig. 3 H). Here, different linear slopes at the beginning (0–15 s) and at the end (30–40 s) of the image sequence become visible. We then calculated the instantaneous velocity V_k (see Section S.9 in the Supporting Material) of the microtubule (Fig. 3 I). The low noise in the curve representing the instantaneous velocity indicates the high precision in our 2D tracking of microtubules.

CONCLUSION

We have developed an algorithm capable of localizing the centerlines and the tips of curved filaments with nanometer precision. Instead of fitting 1-D functions perpendicular to the filament (18,19), we implemented a Gaussian wall model that does not require any image transformation. Therefore, the localization precision of the centerline does intrinsically not depend on the filament orientation (see Section S.7 in the Supporting Material). Furthermore, the tracking of filament tips and filament crossings with nanometer precision have not been reported previously. We created a MATLAB software package called Fluorescence Image Evaluation Software for Tracking and Analysis (FIESTA) (see the MATLAB source code in the Supporting Material). This package includes our filament tracking algorithm, state-of-the-art single particle tracking, and a MATLAB user interface for initialization and further analysis, making it a useful tool for image analysis in many applications. In particular, tracking the 2D movement of motor-proteins on their filaments proves to be a unique tool for studying the function of these molecular machines. Because the single particle tracking is not limited to QDs, labeling motor-proteins with fluorescent beads or gold nanoparticles will improve the time resolution of the experiment while maintaining nanometer localization precision. Combined with methods to measure nanometer heights above substrate surfaces, such as fluorescence interference contrast (34) or parallax (36), our algorithm presents a promising tool for optical 3D-nanometry, not only applicable to cytoskeletal, but also DNA/RNA and other filaments.

SUPPORTING MATERIAL

Nine sections, six figures, and references, as well as the MATLAB source code, are available at [http://www.biophysj.org/biophysj/supplemental/S0006-3495\(11\)00467-X](http://www.biophysj.org/biophysj/supplemental/S0006-3495(11)00467-X). Additional documentation on the usage of FIESTA is available at <http://www.bcube-dresden.de/fiesta>.

We thank C. Bräuer for technical support; D. Naumburger for preparation of the BCCP-rKin430GFP; C. Martin for help with microtubule depolymerization; T. Korten, Y. Kalaidzidis and J. Howard for fruitful discussions; and C. Gell, B. Nitzsche and R. Schneider for comments on the manuscript.

This work was supported by the European Research Council (starting grant 242933), the European Commission (FP7) under the contract MONAD (NMP4-SL-2009-228971), the Deutsche Forschungsgemeinschaft (Heisenberg Professorship and grant DI 1226/3), and the Max-Planck-Society.

REFERENCES

- Cheezum, M. K., W. F. Walker, and W. H. Guilford. 2001. Quantitative comparison of algorithms for tracking single fluorescent particles. *Biophys. J.* 81:2378–2388.
- Thompson, R. E., D. R. Larson, and W. W. Webb. 2002. Precise nanometer localization analysis for individual fluorescent probes. *Biophys. J.* 82:2775–2783.
- Yildiz, A., and P. R. Selvin. 2005. Fluorescence imaging with one nanometer accuracy: application to molecular motors. *Acc. Chem. Res.* 38:574–582.
- Leduc, C., F. Ruhnow, ..., S. Diez. 2007. Detection of fractional steps in cargo movement by the collective operation of kinesin-1 motors. *Proc. Natl. Acad. Sci. USA.* 104:10847–10852.
- Patterson, G., M. Davidson, ..., J. Lippincott-Schwartz. 2010. Superresolution imaging using single-molecule localization. *Annu. Rev. Phys. Chem.* 61:345–367.
- Kron, S. J., and J. A. Spudich. 1986. Fluorescent actin filaments move on myosin fixed to a glass surface. *Proc. Natl. Acad. Sci. USA.* 83:6272–6276.
- Howard, J., A. J. Hudspeth, and R. D. Vale. 1989. Movement of microtubules by single kinesin molecules. *Nature.* 342:154–158.
- Nitzsche, B., V. Bormuth, ..., S. Diez. 2010. Studying kinesin motors by optical 3D-nanometry in gliding motility assays. *Methods Cell Biol.* 95:247–271.
- Fujiwara, I., S. Takahashi, ..., S. Ishiwata. 2002. Microscopic analysis of polymerization dynamics with individual actin filaments. *Nat. Cell Biol.* 4:666–673.
- Mennella, V., G. C. Rogers, ..., D. J. Sharp. 2005. Functionally distinct kinesin-13 family members cooperate to regulate microtubule dynamics during interphase. *Nat. Cell Biol.* 7:235–245.
- Homsher, E., F. Wang, and J. R. Sellers. 1992. Factors affecting movement of F-actin filaments propelled by skeletal muscle heavy meromyosin. *Am. J. Physiol.* 262:C714–C723.
- Work, S. S., and D. M. Warshaw. 1992. Computer-assisted tracking of actin filament motility. *Anal. Biochem.* 202:275–285.
- Chisena, E. N., R. A. Wall, ..., G. Holzwarth. 2007. Speckled microtubules improve tracking in motor-protein gliding assays. *Phys. Biol.* 4:10–15.
- Hamelink, W., J. G. Zegers, ..., T. Blangé. 1999. Path reconstruction as a tool for actin filament speed determination in the in vitro motility assay. *Anal. Biochem.* 273:12–19.
- Li, H., T. Shen, ..., X. Huang. 2009. Automated actin filament segmentation, tracking and tip elongation measurements based on open active contour models. *Proc. IEEE Int. Symp. Biomed. Imaging.* 2009:1302–1305.
- Käs, J., H. Strey, ..., E. Sackmann. 1993. Direct measurement of the wave-vector-dependent bending stiffness of freely flickering actin filaments. *Europhys. Lett.* 21:865–870.
- Brangwynne, C. P., G. H. Koenderink, ..., D. A. Weitz. 2007. Bending dynamics of fluctuating biopolymers probed by automated high-resolution filament tracking. *Biophys. J.* 93:346–359.
- Danuser, G., P. T. Tran, and E. D. Salmon. 2000. Tracking differential interference contrast diffraction line images with nanometre sensitivity. *J. Microsc.* 198:34–53.
- Demchouk, A., M. Gardner, and D. Odde. 2011. Microtubule tip tracking and tip structures at the nanometer scale using digital fluorescence microscopy. *Cell. Mol. Bioeng.* 1–13.
- Hancock, W. O., and J. Howard. 1998. Processivity of the motor protein kinesin requires two heads. *J. Cell Biol.* 140:1395–1405.
- Rogers, K. R., S. Weiss, ..., R. Cross. 2001. KIF1D is a fast non-processive kinesin that demonstrates novel K-loop-dependent mechanochemistry. *EMBO J.* 20:5101–5113.
- Berliner, E., H. K. Mahtani, ..., J. Gelles. 1994. Microtubule movement by a biotinylated kinesin bound to streptavidin-coated surface. *J. Biol. Chem.* 269:8610–8615.
- Helenius, J., G. Brouhard, ..., J. Howard. 2006. The depolymerizing kinesin MCAK uses lattice diffusion to rapidly target microtubule ends. *Nature.* 441:115–119.
- Gell, C., V. Bormuth, ..., J. Howard. 2010. Microtubule dynamics reconstituted in vitro and imaged by single-molecule fluorescence microscopy. *Methods Cell Biol.* 95:221–245.
- Korten, T., and S. Diez. 2008. Setting up roadblocks for kinesin-1: mechanism for the selective speed control of cargo carrying microtubules. *Lab Chip.* 8:1441–1447.
- Nyquist, H. 2002. Certain topics in telegraph transmission theory (Reprinted from Transactions of the A. I. E. E., February, pg 617–644, 1928). *Proc. IEEE.* 90:280–305.
- Toprak, E., H. Balci, ..., P. R. Selvin. 2007. Three-dimensional particle tracking via bifocal imaging. *Nano Lett.* 7:2043–2045.
- Lam, L., S. W. Lee, and C. Y. Suen. 1992. Thinning methodologies—a comprehensive survey. *IEEE Trans. Pattern Anal. Mach. Intell.* 14:869–885.
- Coleman, T. F., and Y. Li. 1996. An interior trust region approach for nonlinear minimization subject to bounds. *SIAM J. Optim.* 6:418–445.
- Coleman, T. F., and Y. Li. 1994. On the convergence of interior-reflective Newton methods for nonlinear minimization subject to bounds. *Math. Program.* 67:189–224.
- Levenberg, K. 1944. A method for the solution of certain problems in least squares. *Q. Appl. Math.* 2:164–168.
- Marquardt, D. W. 1963. An algorithm for least-squares estimation of nonlinear parameters. *J. Soc. Ind. Appl. Math.* 11:431–441.
- Chetverikov, D., and J. Verestói. 1999. Feature point tracking for incomplete trajectories. *Computing.* 62:321–338.
- Nitzsche, B., F. Ruhnow, and S. Diez. 2008. Quantum-dot-assisted characterization of microtubule rotations during cargo transport. *Nat. Nanotechnol.* 3:552–556.
- Desai, A., S. Verma, ..., C. E. Walczak. 1999. Kin I kinesins are microtubule-destabilizing enzymes. *Cell.* 96:69–78.
- Sun, Y., O. Sato, ..., Y. E. Goldman. 2010. Single-molecule stepping and structural dynamics of myosin X. *Nat. Struct. Mol. Biol.* 17:485–491.